IEEE Access
Multidisciplinary | Rapid Review | Open Access Journal

Received 10 June 2022, accepted 22 July 2022, date of publication 29 July 2022, date of current version 5 August 2022.

Digital Object Identifier 10.1109/ACCESS.2022.3195032

RESEARCH ARTICLE

Multiparameter Influence Analysis of the Target Spot Power Distribution of Airborne Laser

LE LIU[1,2], CHENYANG XU[1], WENBIN ZENG[1], BAOKU LI[1,2], JIN GUO[1], AND SHENG CAI[1]

[1]Changchun Institute of Optics, Fine Mechanics and Physics, Chinese Academy of Sciences, Changchun 130033, China
[2]University of Chinese Academy of Sciences, Beijing 100049, China

Corresponding author: Sheng Cai (caisheng@ciomp.ac.cn)

This work was supported in part by the Science and Technology Development Plan of Jilin Province under Grant 20210203151SF; and in part by the Youth Innovation Promotion Association, Chinese Academy of Sciences (CAS), under Grant 2019226.

ABSTRACT With the continuous improvement of the power and miniaturization of high-energy laser weapons, the airborne laser may become the active defense weapon of the next-generation fighter. However, in order to achieve hard damage to the target, there has been a lack of comprehensive quantitative method as a reference in the parameter design of airborne laser. This paper establishes the high-altitude, slope-down, and short-range laser transmission process models based on the laser transmission simulation platform Easylaser to analyze the effect of multiple parameters of airborne laser weapon on the power distribution to the target spot. The simulation results show that the laser power, wavelength, laser emission aperture, tracking accuracy, and transmission distance have significant impact on the power distribution to the target spot, whereas the atmospheric mode, slanted angle, and adaptive optics almost no impact on that. On the basis of the simulation results, the response sensitivity of some parameters' variations to the power distribution to the target spot are analyzed. The response sensitivity variations of the tracking accuracy and transmission distance to the target spot power density varies greatly, while the response sensitivity variations of the laser power and emission aperture to the target power density varies little. These quantifiable outcomes can provide a basis for parameter optimization of airborne laser in the future.

INDEX TERMS Airborne laser, laser transmission, power distribution to the target spot, power density, sensitivity analysis.

I. INTRODUCTION

As the next-generation important alternative self-defense weapon system, the airborne laser weapon has the preponderances of deep magazine, instant engagement, in high-altitude operations, and makes full use of the advantages of high-altitude atmospheric cleanliness to improve the target spot power density [1]. Airborne laser weapons may intercept incoming missiles and bring revolutionary changes to future air combat, however the balance between the volume, weight, and power of laser weapons is still an intractable problem [2]. The SHIELD project in the United States focuses on the development of a compact airborne laser weapon system suitable for airborne platform mounting and energy consumption constraints. It plans to conduct a prototype test on a fighter jet in 2024.

The difficulties airborne laser weapons faced are not only the conflict between laser power and platform load, but also other important aspects such as beam control technology [3], [4]. The beam control system consists of beam director, fast tilt mirror, and adaptive deformable mirror, etc., which requires high-precision tracking and aiming, laser energy control, and laser beam shaping functions [5]. In order to deform the missile shell material, destroy the mechanical structure, melt or directly vaporize, and burn through, it is necessary to consider the influence of laser power, wavelength, and beam control system parameters like laser emission aperture size, laser transmission slanted angle, and tracking accuracy on the power distribution to the target spot. In the demonstration and design of the airborne laser weapons, the airborne laser system sensitivity analysis of parameters'

The associate editor coordinating the review of this manuscript and approving it for publication was Jahangir Hossain.

variations to the power distribution to the target spot is of great significance.

Maurice C. Azar calculated the power density to the target spot for different laser transmission distances and spot jitter at a height of 15km based on the Tyson formula [6]. The calculation method is simple and effective, but it is less accurate since involves few influencing factors. Antonios Lionis used the WaveTrain and ANCHOR software to analyze the effects of the UAV's airborne laser power, laser launch aperture, combat altitude, flight speed and direction, beam quality, and platform jitter on the peak power density and the power in the bucket (PIB) of ground targets [7]. This method has high calculation accuracy, but the calculation speed is limited. Megan p.Melin used modeling and simulation software HEELEOS embed a laser transmission fast calculation tool SHARE to analyze the response sensitivity of the airborne laser weapon system parameters' variations, such as slope distance, laser power, wavelength, and laser emission aperture to the PIB [8]. The simulation scene was aimed at the ground target, but the values related to power of the target spot was not included. Xu *et al.* used empirical formulas to analyze the influence of different laser power, apertures, transmission distances, and atmospheric modes on the power density to the target spot [9]. The method is efficient, but it is only a rough estimate of the power density to the target spot. Yun *et al.* proposed an improved 4-level guidance system design method to evaluate the impact of system design parameters on UAV mission effectiveness. In summary, the existing studies mainly focuses on the system design method of the airborne laser, whereas the calculation methods about the power density to the target spot are relatively rough and imperfection [10].

The laser propagation process in the atmosphere is also an important research interest. Zhao *et al.* used a 4-D laser transmission program to simulate the impact of atmosphere on high-energy laser, and compared it with the laser transmission measured in the field [11]. Yin used a low-cost liquid crystal phase spatial light modulator [12] to load the thermal blooming phase screen to obtain the far-field distorted phase diagram, and used the turbulence simulator [13], [14] to simulate the atmospheric refractive index constant of turbulence. But like most of the previous works, adaptive optics compensation [15], [16] was not considered. Wu *et al.* built a laser transmission process model to study the steady-state thermal blooming effect of different laser beams in the uniform atmosphere based on the laser transmission simulation platform Easylaser [17]. However, the existing works were not applied to the scene of airborne laser striking air targets.

In this paper, a numerical simulation method combining Easylaser with a secondary spot diagnosis calculation program is proposed to analyze the effects of system parameters, transmission path parameters and atmospheric mode on the power distribution to the target spot in the airborne laser high altitude and close-range combat scenario. Easylaser [18], a system-level laser simulation platform which is similar to WaveTrain, is used to build the laser transmission process model with adaptive optics compensation. Secondary spot diagnosis is a new comprehensive method to evaluate the power distribution of the target spot. In order to further study the influence of some parameters on the target power distribution, based on the simulation results, a polynomial fitting and low-order derivation method is used to analyzed the respond sensitivity of some parameters' variations to the power distribution of the target spot.

This article is organized as following. In Section II, the influencing factors of the power distribution to the target spot are introduced. The analysis methods and steps for the effect of multiple parameters on the power distribution to the target spot are given in Section III. In Section IV, the influence of different parameters on the power to the target spot is analyzed. Finally, section V is the conclusion and briefly further development directions.

II. INFLUENCING FACTORS

Success of airborne laser high-altitude interception of incoming missiles depends on many factors. In addition to the obvious factors such as laser power, laser emission aperture, and transmission distance, the interaction between the laser and the atmosphere, which resulting in many linear and nonlinear effects play an important role in the successful interception. Among the nonlinear effects, this paper only considers the thermal blooming effect, ignoring the thermoman and punch-through effect, and the linear effects like atmospheric absorption, scattering, and turbulence effects are considered. Besides, the shock wave effect in the flying combat environment and the thermal effect of the mirror is not considered.

A. ATMOSPHERIC EXTINCTION

In the process of laser transmission in the atmosphere, there are molecules and aerosols that absorb and scatter the incident light, resulting in the loss of laser energy. Specifically, molecules can absorb photons with a certain energy and re-emit photons with lower energy, while aerosols have very little energy absorption and are dominated by scattering. This atmospheric attenuation is related to the laser wavelength and atmospheric physical properties, and mainly exists near the ground and at low altitudes. When the laser is transmitted at high altitude, the attenuation of laser power is small. The formula for laser transmission in a homogeneous atmosphere is given as follow [19].

$$P(\lambda, z) = P_0 e^{-\varepsilon(\lambda) z} \tag{1}$$

where P_0 is the output power of the beam director, $P(\lambda, z)$ is the power after the transmission distance z with specific wavelength λ, and ε is the extinction coefficient. The extinction coefficient consists of four parts.

$$\varepsilon = \alpha_m + \alpha_a + \beta_m + \beta_a \tag{2}$$

where α and β are the absorption coefficient and scattering coefficient. The subscript m represents the molecule, and the subscript a represents the aerosol.

B. ATMOSPHERIC TURBULENCE EFFECTS

When the laser is transmitted through the atmosphere, due to the irregular distribution of refractive index caused by random changes in local temperature and pressure in the atmosphere, the phase and intensity fluctuate randomly, resulting in spot drift, expansion and flickering [20], [21]. A common parameter describing the strength of weak turbulence on a path is the Fried parameter r_0.

$$r_0 = [\frac{2.905}{6.88}\left(\frac{2\pi}{\lambda}\right)^2 \int_{path}^{R} C_n^2(h(z))dz]^2 \tag{3}$$

where z is the transmission distance, λ is the laser wavelength, C_n^2 is the refractive index structure parameter, which can characterize the main parameter of atmospheric turbulence, and it depends on local atmospheric data.

C. THERMAL BLOOMING EFFECT

The thermal blooming effect is that when a high-energy laser transmits in the atmosphere, the laser heats the air to form an equivalent negative lens, and under the impact of lateral wind, a meniscus-shaped spot distribution is formed [22]. Assuming constant atmospheric conditions, we can characterize thermal blooming in terms of so-called dimensionless thermal distortion parameter.

$$N_D \approx \frac{-8\sqrt{2}\pi P n_T \alpha T}{\rho_0 C_P D \lambda V_{mind}} R \tag{4}$$

where P is the laser power, n_T is the change of refractive index with temperature, T is the atmospheric temperature, α is the absorption coefficient, ρ_0 is the atmospheric density, C_P is the atmospheric capacity, D is the beam diameter, V_{mind} is the effective wind speed perpendicular to the beam, and R is the distance between the laser and the target.

D. SPOT JITTER AND BEAM DIFFRACTION

The main function of the beam control system is to point the laser beam precisely at a certain point of the target and maintain it for a period of time. The tracking subsystem in the beam control system consists of a photoelectric sensor and a gyroscope to track the dynamic target, and the beam director guides the weapon towards the target. Small errors are unavoidable during the tracking process.

In the process of laser transmission, the light will deviate from the straight line propagation when encountering obstacles or small holes. Due to the limitation of the aperture of the laser emission system, the divergence angle is

$$\theta_y = 1.22\frac{\lambda}{D_0}Q \tag{5}$$

where D_0 is the laser emission aperture, Q is the quality factor. The spot jitter and beam diffraction need to be considered comprehensively with the atmospheric extinction, turbulence and thermal blooming effects mentioned above.

E. ADPTIVE OPTICS COMPENSATION

The adaptive optics system is used for the phase correction of the laser. The beacon light and the main laser pass through the same atmospheric channel. The Hartmann sensor detects the phase distortion information carried by the beacon light. The deformable mirror and the tilting mirror are used to correct wavefront distortion. On the initial phase of laser emission, a conjugate phase opposite to the phase distortion caused by turbulence and thermal blooming is superimposed in advance. The beacon light aberration detected by the Hartmann sensor is used to solve for the Zernike coefficients [23]:

$$\lambda\lambda \begin{cases} \partial\omega(x,y)/\partial x|_m = x_{c,m}/2\pi f \\ \partial\omega(x,y)/\partial y|_m = y_{c,m}/2\pi f \end{cases} \tag{6}$$

$$\begin{cases} \partial\omega(x,y)/\partial x|_m = \sum_{k=1}^{npl} A_k \partial Z(x,y)/\partial x|_m \\ \partial\omega(x,y)/\partial y|_m = \sum_{k=1}^{npl} A_k \partial Z(x,y)/\partial y|_m \end{cases} \tag{7}$$

where $x_{c,m}$, $y_{c,m}$ are the magnitude of the spot drift of the sub-aperture imaging of the Hartmann sensor, f is the focal length of the sub-aperture, λ is the laser wavelength. $\omega(x, y)$ is the wave aberration, x and y are the abscissa and ordinate perpendicular to the beam, respectively, A_k is the Zernike coefficient, $Z(x, y)$ is the Zernike polynomial, m represents a certain Hartmann sub-aperture. The beam spot shift of the beacon light is measured through the Hartmann sub-aperture, and the polynomial is known data through a look-up table. According to (6) and (7), the Zernike coefficient can be calculated, which is the input to control the tilt and deformable mirror.

III. METHODS AND STEPS

A. MODEL BUILDING

Easylaser contains a variety of component libraries, such as laser source component library, optical component library, atmospheric component library, detection component library, etc., which can easily build a three-dimensional optical path transmission process model. In order to simulate the high-altitude combat of the fighter, the height position of the model component is set to 10km. Laser sources use the ideal Gaussian beam. The laser emission system adopts the classic Cassegrain system to realize the far-field focusing of the continuous laser beam. The adaptive optics module is used to compensate for the atmospheric turbulence and thermal blooming effect. The laser transmission process model is shown Fig. 1.

B. SPOT DIAGNOSIS

Multi frame spot distribution data will be generated after the model runs. The ring radius and power density of the spot that account for 0.8378 and 0.6320 of the total target power are selected as the four indicators of the target spot power

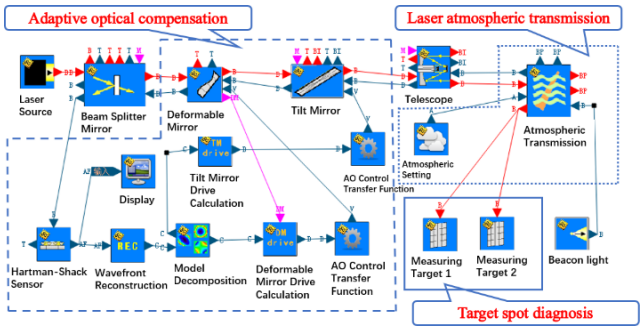

FIGURE 1. Laser transmission process model.

TABLE 1. Laser transmission path, atmospheric setting and target parameters.

	Parameter	Value
Laser transmission path	Transmission distance	4 km
	Combat altitude	10 km
	Slanted angle	45 degrees
Atmosphere	Atmospheric mode	Mid-latitude summer marine type VIS=100 km
	Number of atmospheric stratification（0-10 km）	35
Target	Pixel size	0.049 cm
	Number of pixels	1024 × 1024

distribution.

$$I_{0.8378} = \frac{0.8378 P_{target}}{\pi R_{0.8378}^2} \tag{8}$$

$$I_{0.6320} = \frac{0.6320 P_{target}}{\pi R_{0.6320}^2} \tag{9}$$

where P_{target} is the total power to the target, R is the circle radius of the spot, I is the average power density within the circle radius of the spot. The subscript 0.8378 is the ratio of the power in the first dark ring of Airy spot to the total target power, and the subscript 0.6320 is the ratio of the power within the beam waist radiu to the total target power.

Easylaser lacks a multi-frame spot diagnosis due to spot jitter. It is necessary to perform a secondary spot diagnosis on the spot result. We select the ring radius and ring power density data of the first 200 frames as the analysis object, and the frame frequency is 1000Hz. Through the Matlab programming software, we only select three different power ratios of ring radius and power density for each frame as the basic data since the amount of data is large. Three different power ratios are 0.9500, 0.8378 and 0.6320, respectively. The above result data are processed to display the power distribution after averaging multiple frames of spots. The four indicators of the above ideal beam are still used in the secondary spot diagnosis involving spot jitter, and shown in Fig. 2. The mesh size is 0.0025 cm, which is smaller than the target pixel size. The pixel size of the target is shown in Table 1.

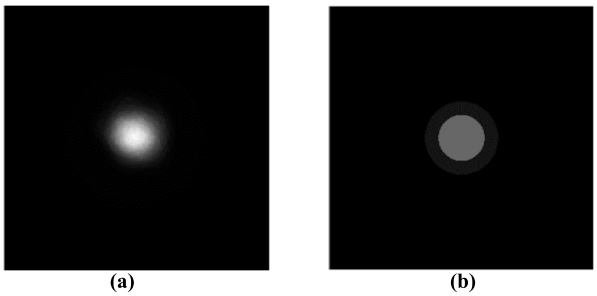

FIGURE 2. Spot power distribution before and after secondary diagnosis. (a) Multi-frame to target spot distribution (before). (b) Secondary spot diagnosis (after).

C. SENSITIVITY ANALYSIS

Sensitivity analysis can reflect the influence degree of input variables on output variables. If a function $f(x)$ can be derived, its first-order sensitivity can be expressed as

$$S^{\text{ratio}}_{para(\Delta x)}(x) = \frac{\partial f(x)}{\partial x_i} \tag{10}$$

where x_i is the set of parameter variables, $S^{\text{ratio}}_{para(\Delta x)}(x)$ is called the first-order differential sensitivity of $f(x)$ to the parameter x_i, the subscript Δx is the parameter increment, and superscript ratio represents the ratio of power to the total target power.

In the process of numerical simulation, a sufficiently large and reasonable set of parameters variables are selected. The continuous parameter response curve is obtained by means of low-order polynomial fitting. Because the high-order polynomial fitting will cause great fluctuation to the derivative function curve, the fourth-order polynomial fitting is chosen, and the polynomial coefficients will be given in Table 2. The first-order response sensitivity to parameter increments Δx can be represented by the derivative function $S^{\text{ratio}}_{para(\Delta x)}(x)$. The derivative function can be obtained by derivation according to Table 2. When comparing the response sensitivity of each parameter's variation to the target power distribution, it largely depends on the parameter incrementΔx.

IV. DATA RESULT ANALYSIS

The high-energy laser passes through the laser emission system and the atmosphere to achieve far-field focusing of the spot. The wavefront distortion caused by turbulence and thermal blooming can be corrected through the adaptive optical components. In this process, we assume that the system has an automatic focusing function. The focus position of the laser emission system is always located at the target, and coincides with the position of the beam waist of the ideal Gaussian beam.

In the basic model of laser transmission, the detailed parameter settings are shown in Table 1 and Table 3.

Note: 1) The laser source power in the Table 2 is 60 kw, but the actual output power is 44.8 kw, the power loss is mainly caused by the beam splitter and the central obscuration of the

TABLE 2. Polynomial fitting coefficient of influence of different parameters on power distribution of target spot. Note: To ensure that the data is clearly displayed with high precision, "e value" will represent "$\times 10^{value}$", e.g., "e-07" represent "$\times 10^{-7}$". "Laser source power: 30:2:90 kw" indicates that the laser power is between 30 – 90 kw, its increment is 2, and the format of the other variable intervals is similar.

Polynomial order	4	3	2	1	0
Polynomial coefficient (laser source power: 30:2:90 kw)					
$R_{0.8378}$	-8.535724423923148e-10	3.752193668590394e-07	-4.324383059747034e-05	0.003324570985966	1.843832907308948
$R_{0.6320}$	8.686799192420438e-11	3.415548725982047e-08	-6.360606559164464e-06	0.001648671088064	1.144146612054426
$I_{0.8378}$	-9.796795875398707e-07	-4.074681646429198e-04	0.001298038490474	52.779704976068250	70.480496366673300
$I_{0.6320}$	-1.786920923488125e-05	0.003942882977603	-0.525002205918306	1.230816520148125e+02	-1.021570690387515e+02
Polynomial coefficient (the laser emission aperture: 0.15:0.01:0.65 m)					
$R_{0.8378}$	-18.499818483663480	12.650723142037354	13.250239642353794	-14.949532249208369	5.464465682341213
$R_{0.6320}$	48.618509771290450	-99.514846585840540	77.612057633816850	-28.269486046486510	5.240231098749771
$I_{0.8378}$	7.414228837846880e+04	-1.355959927125177e+05	8.496709050195172e+04	-1.242632154100029e+04	1.322518425626799e+03
$I_{0.6320}$	9.885404804268532e+04	-1.736109521936324e+05	9.516901703219005e+04	-1.968168849955516e+03	1.906278217644242e+02
Polynomial coefficient (the tracking accuracy: 0:0.1:5 urad)					
$R_{0.8378}$	0.001816618738196	-0.022451912674554	0.107471166096283	0.209600010191074	1.256522454357236
$R_{0.6320}$	0.001491811369857	-0.022942091077237	0.132927522635154	6.168610060128973e-04	0.854715226802183
$I_{0.8378}$	-9.618934452616110	50.180447870820640	3.442184459020115e+02	-3.102417171369285e+03	7.679073868322977e+03
$I_{0.6320}$	-63.098611466121405	6.776437108519536e+02	-1.930477696561780e+03	-1.589191804406023e+03	1.260285927024281e+04
Polynomial coefficient (the transmission distance: 2000:10:7000 m)					
$R_{0.8378}$	8.887601653717670e-16	-1.598668420257465e-11	1.082762392113866e-07	2.000099391835040e-04	0.231550244108690
$R_{0.6320}$	1.891172712005285e-17	-4.064037328642200e-13	9.406110610187626e-09	2.733954832024782e-04	0.004710068042879
$I_{0.8378}$	6.951918327149352e-11	-1.479909823275335e-06	0.011838174610261	-42.968382088212600	6.245697489542855e+04
$I_{0.6320}$	1.467424946745074e-10	-3.109784594589721e-06	0.024726599659949	-89.000859912639570	1.277287469479806e+05

laser emission system. A small fraction of the power loss is due to mirror absorption. 2) This model uses a coaxial adaptive optics system, which may cause the central obscuration area to be larger than the sub-aperture size of the Hartmann sensor without central obstruction, making the central area of the Hartmann sensor without light. Therefore, the laser

TABLE 3. Airborne laser system and parameters.

	Parameter	Value
Laser power	Laser source power	60 kw
	Actual output power	44.8265 kw
	Main laser wavelength	1.064 um
	Beacon Light Wavelength	0.532 um
Laser launch system (Classic Cassegrain System)	Tracking accuracy	2 urad
	Primary mirror curvature Radius	2.21 m
	Secondary Mirror Curvature Radius	0.36 m
	Central obscuration	3/20
	Laser emission aperture	0.4 m
Adaptive optics	Beam splitter ratio	9:1
	Hartmann lateral element number of spot interior	10
	Deformable mirror driver turns spot interior (arrangement)	6 (triangular)

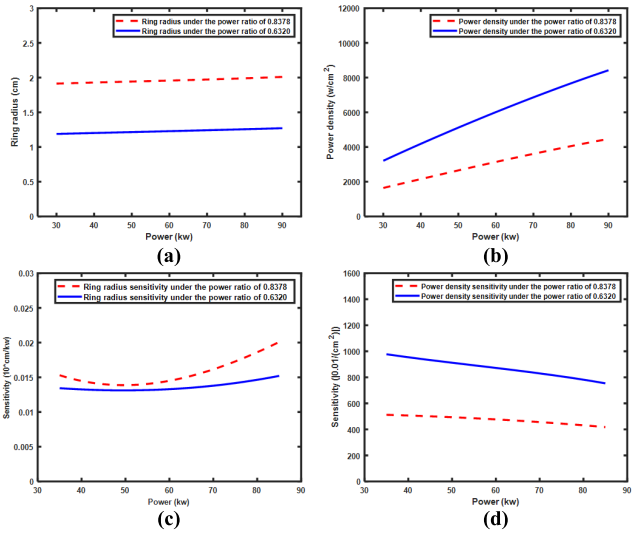

FIGURE 3. The effect of laser power on the power distribution to the target spot. (a) The effect of laser power on the ring radius to the target spot. (b) The effect of laser power on the power density to the target spot. (c) The response sensitivity of the laser power's variations to the spot ring radius (parameter increment 10 kw). (d) The response sensitivity of the laser power's variations to the spot power density (parameter increment 10 kw).

emission system in this model needs to choose an appropriate central obscuration ratio to avoid the above problem.

A. INFLUENCE OF LASER POWER ON THE POWER DISTRIBUTION TO THE TARGET SPOT

Referring to the 2018 version of the US airborne laser weapons roadmap, the first phase of the airborne laser weapon system, based on tens of kilowatts of high-energy airborne lasers, demonstrates damage to infrared-guided air-to-air missiles [24]. In 2021, Lockheed Martin had delivered the first airborne high-energy laser weapon system [25]. According to US media reports, its power is about 60 kw. Therefore, in the selection of the power parameter, the power of the laser transmission process model is assumed to be 60±30 kw. Compared with the airborne laser weapon test in Israel in 2021, the power level of airborne laser weapon is much higher, and the working distance will be farther.

In order to study the effect of the airborne laser power on the power distribution to the target spot, we change the power of the main laser in the laser transmission process model, and other parameters are consistent with Table 1 and Table 3. The effect of laser power on the power distribution to the target spot is shown in Fig. 3.

When the main laser power is low, the spot ring radius increases approximately linearly with the power. When the main laser power is higher, the curve of the response sensitivity of the laser power's variation to the spot ring radius becomes steeper, as shown in Fig. 3(c). The response sensitivity curve of the laser power's variation to the spot power density is related to the response sensitivity curve of the laser power's variation to the spot ring radius. With the increase of laser power, the growth rate of spot power density slows down shown in Fig. 3 (d). The reason for the slowing down is that with the increase of laser power, the thermal distortion parameter gradually increases, and the adaptive optics correction ability gradually weakens, which cannot well compensate the phase fluctuation caused by thermal blooming. In order to increase the power density of the target spot, although the growth rate of the spot power density is slowed down, there is still a large space for the improvement of the spot power density by increasing the power. Therefore, within the range of the above power variation, there is no need to consider a situation, that is, when the laser power is increased, the thermal distortion parameter gradually increases according to formula (4), and the adaptive correction capability is weakened, resulting in the maximum value of the power density to the target spot [26].

Within the variation range of the laser power, for each increase of 10 kw, the power density under the power ratio of 0.8378 increases by 418-512 w/cm^2, and the power density under the power ratio of 0.6320 increases by 754-978 w/cm^2. When the laser power of the basic model is 60kw,

$$S^{0.8378}_{laser\ source\ poewer(10\mathrm{kw})} = 476\mathrm{w}/\mathrm{cm}^2,$$
$$S^{0.6320}_{laser\ source\ poewer(10\mathrm{kw})} = 863\mathrm{w}/\mathrm{cm}^2.$$

These data need to meet the basic preconditions in Table 1 and Table 3. Similar to the above, we all use the control single variable method to analyze the influence of different parameters on the power distribution to the target spot in the following other parameter analysis.

B. THE INFLUENCE OF LASER EMISSION APERTURE ON THE POWER DISTRIBUTION TO THE TARGET SPOT

In the laser transmission process, the larger the laser emission aperture, the smaller the spot size caused by diffraction. The laser emission aperture is smaller than the diameter of the laser launch turret. At present, the diameter of most

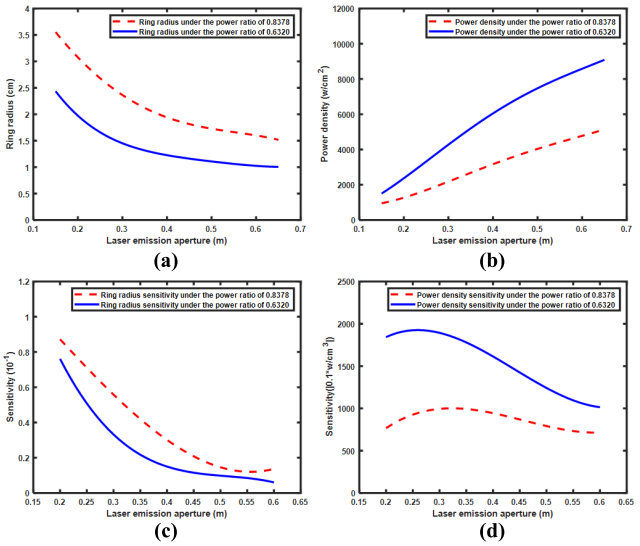

FIGURE 4. The effect of laser emission aperture on the power distribution to the target spot. (a) The effect of laser emission aperture on the ring radius to the target spot. (b) The effect of laser emission aperture on the power density to the target spot. (c) The response sensitivity of the laser emission aperture's variation to the spot ring radius (parameter increment 0.1m). (d) The sensitivity response of the laser emission aperture's variation to the spot power density (parameter increment 0.1 m).

photoelectric turrets is slightly larger than 0.4m, but there are a few cases, such as the MTS-B photoelectric sighting system of Raytheon Company, the diameter of the photoelectric turret is 0.559 m [27]. Taking into account other conditions, it is necessary to choose a larger diameter as much as possible. Therefore, this paper chooses 0.4±0.25 m for the laser emission aperture. The effect of the laser emission aperture on the power distribution to the target spot is shown in Fig. 4.

According to formula (5), the relation function between the target spot ring radius and the laser emission aperture is an inverse proportional function. Its shape is a hyperbola distributed in the first and third quadrants. As shown in Fig. 4 (a), the variation curve of the spot ring radius with the laser emission aperture is approximately consistent with a part of the hyperbola after moving downward for a certain range. The range of downward movement is numerically equal to the spot ring radius without considering the aperture diffraction. However, the relationship function between the power density and the spot ring radius is an approximate inverse proportional function again. The variation of power density with laser emission aperture is shown in Fig. 4 (b), and the magnitude of its variation is shown in Fig. 4 (d). There is a certain extreme point in the response sensitivity of the laser emission aperture's variation to the target spot power density under two different power ratios. The extreme point cannot be explained from the point of the above mathematical formula, but it can be obtained that the response sensitivity of the laser emission aperture's variation to the target spot power density is a decreasing function. In Fig. 4 (d), there is an increase in the curve. The reason is that the above-mentioned inverse proportional function ignores the influence of the nonlinear thermal blooming effect. The response sensitivity of the laser emission aperture's variation to the target spot power density caused by the thermal blooming is an increasing function. It is combined with the above-mentioned decreasing function to explain the curve change in Fig. 4 (d). The response sensitivity of the laser emission aperture's variation to the ring radius, if the thermal blooming is also ignored, is a negative second-order function of the aperture, which is approximately consistent with the curve change in Fig. 4 (c). However, the variation curve of the ring radius to the target spot under the two different power ratios is quite different. It mainly because the thermal blooming causes the target spot power of the inner ring move to the outer ring, which increases the ring radius to the target spot under the power ratio of 0.6320. This can also be seen in Fig. 4 (a).

In the design of airborne laser weapons, the response sensitivity under the power ratio of 0.8378 is larger when the aperture is 0.32 m. Within the variation range of the laser emission aperture, for each increase of 0.1m, the power density under the power ratio of 0.8378 increases by 714-1002 w/cm^2, and the power density under the power ratio of 0.6320 increases by 1014-1926w/cm^2. When the laser emission aperture of the basic model is 0.4m,

$$S^{0.8378}_{laser\ emission\ aperture(0.1m)} = 944\mathrm{w}/\mathrm{cm}^2,$$
$$S^{0.6320}_{laser\ emission\ aperture(0.1m)} = 1614\mathrm{w}/\mathrm{cm}^2.$$

C. THE INFLUENCE OF LASER EMISSION SYSTEM TRACKING ACCURACY ON THE POWER DISTRIBUTION TO THE TARGET SPOT

In modern warfare, the role of high-precision target positioning and tracking, precision guidance and other technologies based on airborne platforms in information warfare is becoming more and more prominent. With the development of directed energy weapons, higher requirements are put forward for accurate guidance equipment. At present, the tracking accuracy of the MX-25D electro-optical sighting system of Canadian WESCAM company and the SPECTRO XR electro-optical sighting system of Israel Elbit company can reach 3 urad. In unpublished reports, its tracking accuracy is even higher. The tracking accuracy parameter in this paper is 0-5 urad. The effect of the tracking accuracy on the power distribution to the target spot is shown in Fig. 5.

As the tracking accuracy increases, the response sensitivity curve of the tracking accuracy's variation to the target spot ring radius gradually slows down and eventually stable, as shown in Fig. 5 (c). The trend of this curve is more intuitive as shown in Fig. 5 (a). The reason is that the spot itself has a certain size when the tracking accuracy is not considered. When the tracking accuracy is close to 0 urad, the ratio of the spot ring radius to the ring radius caused by the tracking accuracy is larger. This relative ratio gradually decreases as the tracking accuracy increases. When tracking accuracy is above 3 urad, the relative ratio becomes smaller, which

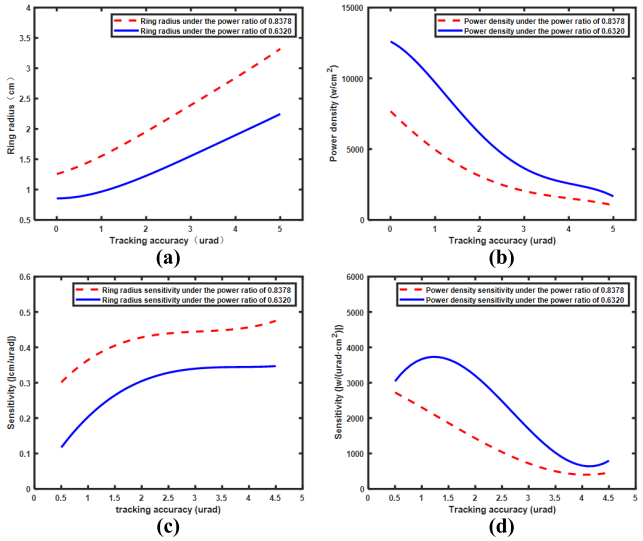

FIGURE 5. The effect of tracking accuracy on the power distribution to the target spot. (a) The effect of tracking accuracy on the ring radius to the target spot. (b) The effect of tracking accuracy on the power density to the target spot. (c) The response sensitivity of the tracking accuracy's variation to the spot ring radius (parameter increment 1 urad). (d) The response Sensitivity of the tracking accuracy's variation to the spot power density (parameter increment 1 urad).

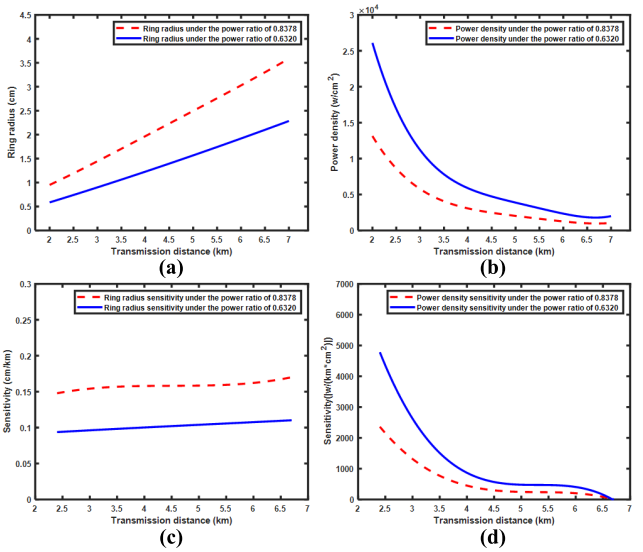

FIGURE 6. The effect of laser transmission distance on the power distribution to target spot. (a) The effect of laser transmission distance on the ring radius to the target spot. (b) The effect of laser transmission distance on the power density to the target spot. (c) The response sensitivity of the laser transmission distance's variation to the spot ring radius (parameter increment 300 m). (d) The response sensitivity of the laser transmission distance's variation to the spot power density (parameter increment 300m).

results in the spot approximated as a point. At this time, the response sensitivity of the tracking accuracy's variation to the ring radius tends to a constant value. The variation curve in Fig. 5(d) is related to the variation curve in Fig. 5(c).

Under the above premise, the response sensitivity of the tracking accuracy's variation to the power density under the power ratio of 0.6320 has a maximum value between the tracking accuracy of 1 and 1.5 urad. Within the variation range of the tracking accuracy, for each increase of 1 urad, the power density under the power ratio of 0.8378 increases by 402-2725 w/cm^2, and the power density under the power ratio of 0.6320 increases by 641-3731 w/cm^2.When the tracking accuracy of the basic model is 2urad,

$$S^{0.8378}_{\text{tracking accuracy}(2urad)} = 1431\mathrm{w}/\mathrm{cm}^2,$$
$$S^{0.6320}_{\text{tracking accuracy}(2urad)} = 3199\mathrm{w}/\mathrm{cm}^2.$$

D. THE INFLUENCE OF LASER TRANSMISSION DISTRANCE ON THE POWER DISTRIBUTION TO THE TARGET SPOT

Referring to the airborne high-energy laser weapon demonstration prototype carried out by the Israeli Air Force in June 2021, which used a about 10 kw laser weapon to shoot down the Sky Striker cruise missile to 1 km away [28]. In the laser transmission simulation model of this paper, the 60 kw laser power can shoot down the missile at a longer distance. Shells of different materials and thicknesses have different damage thresholds [29]. At present, high-power laser damage is mainly melting. Normally, laser spot stays for 3s to burn through a 10 mm thick steel missile casing, and the power density is about 2-5 $\mathrm{kw}/\mathrm{cm}^2$. Considering the surface reflection and other factors, the laser transmission distance corresponding to the target power density required to melt through the target is about 3∼5km. This paper is based on the transmission distance of 4km, and the variation range is 2 -7 km. The effect of the transmission distance on the power distribution to the target spot is shown in Fig. 6.

As shown in Fig. 6(a), the relationship between the spot ring radius and the transmission distance is approximately linear. As shown in Fig. 6(c), there are only minor fluctuations with a slight upward trend. The reason is that the target spot itself has a certain size. At the same time, the beams converge at different distances, and its aberration, turbulence, thermal blooming, adaptive optics compensation, etc. may cause a slight disturbance of the response sensitivity curve of the transmission distance's variation to the ring radius. In Fig. 5(b), the variation curve of the spot ring radius with the transmission distance is approximately consistent with a part of the hyperbola after moving a range to the left. The variation curve in Fig. 5(d) is related to the variation curve in Fig. 5(c).

Under the above premise, the response sensitivity of the transmission distance's variation to the power density can be divided into two sections. Within 3.5 km, the response sensitivity of the transmission distance to the target spot power density is greater, as the transmission distance is smaller, the target spot power density rises rapidly. Beyond 3.5 km, the response sensitivity of the transmission distance's variation to the power density is relatively small, for each increase of 300m, the power density under the power ratio of 0.8378 does not exceed $1466\mathrm{w}/\mathrm{cm}^2$. The power density under the power

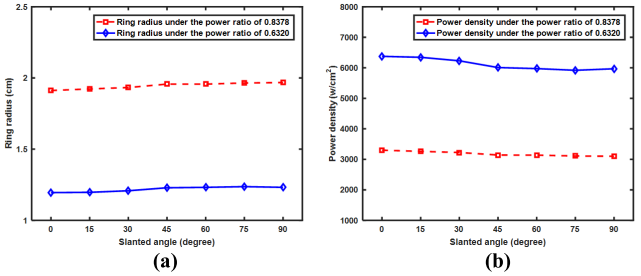

(a) (b)

FIGURE 7. The effect of the laser transmission slanted angle on the power distribution to the target spot. (a) The effect of the transmission distance slanted angle on the ring radius to the target spot. (b) The effect of the transmission slanted angle on the power density to the target spot.

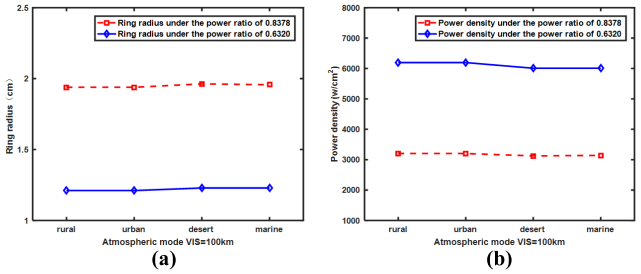

(a) (b)

FIGURE 8. The effect of atmospheric mode on the power distribution to Target spot. (a) The effect of atmospheric mode on the ring radius to the target spot. (b) The effect of atmospheric mode on the power density to the target spot.

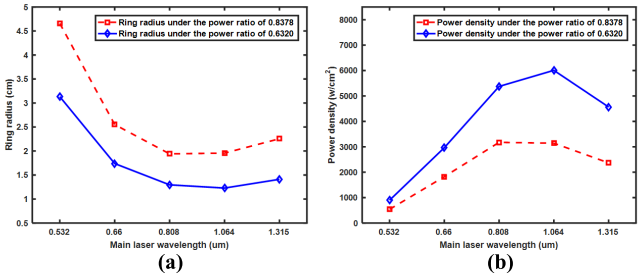

(a) (b)

FIGURE 9. The effect of the main laser wavelength on the power distribution to the target spot. (a) The effect of the main laser wavelength on the ring radius to the target spot. (b) The effect of the main laser wavelength on the power density to the target spot.

ratio of 0.6320 does not exceed 778w/cm^2. When the transmission distance of the basic model is 4km,

$$S^{0.8378}_{transmission\ distance(300m)} = 455\text{w}/\text{cm}^2,$$
$$S^{0.6320}_{transmission\ distance(300m)} = 859\text{w}/\text{cm}^2.$$

E. THE INFLUENCE OF LASER TRANSMISSION SLANTED ANGLE ON THE POWER DISTRIBUTION TO THE TARGET SPOT

During the laser transmission process, if the transmission distance is constant, with the increase of the slanted angle, the laser end is closer to the ground. The C_n^2 in the Fried parameter r_0 of atmospheric turbulence and the V_{mind} parameter in the thermal distortion parameterN_D are related to the altitude. Easylaser uses the phase screen to simulate the atmosphere [30], [31]. The wind speed and direction for each layer of the phase screen are different. The change of the angle between the wind direction and the laser transmission direction makes the power distribution of the target spot more complicated [32]. However, the laser transmission process model in this paper is applied to the airborne laser high-altitude close combat scenario. Atmospheric turbulence and thermal blooming are mainly concentrated in the ground 2 km. Therefore, the influence of atmosphere on laser transmission is not great in this model. The effect of the laser transmission slanted angle on the power distribution to the target spot is shown in Fig. 7.

In Fig. 7, the target spot ring radius increases slightly with the increase of the laser transmission slanted angle. After verification analysis, it is mainly due to thermal blooming effect. In this model, the laser transmission is below 10 km, and the wind speed increases linearly with height. When the target position is low, it is difficult to blow away the air heated by the laser due to the small wind speed, resulting in a larger thermal. However, the power density to the target spot and the ring radius change little with the slanted angle. Due to the small variation of the power density to the target spot, and limited by the calculation time of Easylaser, it is not suitable for sensitivity analysis.

For every 15degrees increase, the maximum relative variation of the power density under the power ratio of 0.8378 does not exceed 3.6%, and the maximum relative variation of the power density under the power ratio of 0.6320 does not exceed 2.6%. The maximum difference in power density under the power ratio of 0.8378 is 407w/cm^2. The maximum difference in power density under the power ratio of 0.6320 is 199w/cm^2.

F. THE INFLUENCE OF ATMOSPHERIC MODE ON POWER DISTRIBUTION TO THE TARGET SPOT

Easylaser has a variety of atmospheric modes, and the atmospheric parameters in each atmospheric mode are divided into conventional, optical, and turbulence parameters. The conventional parameters include pressure, density, temperature, wind speed, and wind direction. Optical parameters including absorption and scattering coefficients of molecules and aerosols. Turbulence parameters include inner and outer dimensions and refractive index structure parameter C_n^2. Each parameter is a profile that varies with altitude. The effect of the atmospheric mode on the power distribution to the target spot is shown in Fig. 8.

Because the atmospheric database in Easylaser is not perfect enough, there is a lack of atmospheric data in fog, rain, etc. In the case of existing atmospheric data, there are only three levels of atmospheric visibility on sunny days in the laser transmission process model. Under the same geographical type, the visibility of 150km and 200km will hardly bring changes to the laser atmospheric transmission. Therefore, we only calculate whether it will affect laser transmission for different regional types.

As shown in Fig. 8, there is a slight decrease in power density to the target for the desert type and the ocean type compared with the rural type and the urban type. The maximum

TABLE 4. Influence of adaptive optics, turbulence and thermal blooming effects on the power distribution to the target spot.

Transmission distance (km)	2	3	4	5	6	7
Spot distribution after adaptive optics compensation						
$R_{0.8378}$ (cm)	0.584	0.899	1.229	1.579	1.915	2.285
$R_{0.6320}$ (cm)	0.949	1.440	1.957	2.499	3.027	3.581
$I_{0.8378}$ (w/cm^2)	26716.230	11267.393	6008.500	3634.410	2463.202	1723.370
$I_{0.6320}$ (w/cm^2)	13402.560	5817.255	3141.957	1923.188	1306.712	930.275
Spot distribution without adaptive optics compensation						
$R_{0.8378}$ (cm)	0.592	0.912	1.258	1.608	1.955	2.333
$R_{0.6320}$ (cm)	0.955	1.459	1.991	2.544	3.088	3.659
$I_{0.8378}$ (w/cm^2)	25999.821	10939.944	5820.411	3502.242	2362.889	1652.752
$I_{0.6320}$ (w/cm^2)	13253.523	5669.109	3041.582	1854.843	1255.039	891.126
Spot distribution without turbulence and thermal blooming effects						
$R_{0.8378}$ (cm)	0.579	0.867	1.262	1.442	1.736	2.024
$R_{0.6320}$ (cm)	0.941	1.413	2.004	2.345	2.827	3.288
$I_{0.8378}$ (w/cm^2)	27210.462	12114.121	6779.093	4354.958	2995.682	2196.548
$I_{0.6320}$ (w/cm^2)	13631.162	6038.522	3395.996	2182.988	1497.850	1103.372
The relative difference of the power density to the target spot with and without adaptive optics compensation						
$I_{0.8378}$	2.76%	2.99%	3.23%	3.77%	4.25%	4.27%
$I_{0.6320}$	1.12%	2.61%	3.30%	3.68%	4.12%	4.39%
The relative difference of the power density to the target spot with and without turbulence and thermal blooming effects						
$I_{0.8378}$	4.68%	9.69%	14.14%	19.58%	21.20%	24.76%
$I_{0.6320}$	2.77%	6.12%	10.44%	15.03%	16.21%	19.24%

relative variation of the power density under the power ratio of 0.8378 does not exceed 3.0%, and the maximum relative variation of the power density under the power ratio of 0.6320 does not exceed 2.4%. The maximum difference in power density under the power ratio of 0.8378 is $167w/cm^2$. The maximum difference in power density under the power ratio of 0.6320 is $78w/cm^2$. Since the variation of the target spot power density is very small, and the atmospheric mode is the transmission environment of the laser, it is not suitable for sensitivity analysis.

G. THE INFLUENCE OF MAIN LASER WAVELENGTH ON POWER DISTRIBUTION TO THE TARGET SPOT

Atmospheric extinction, turbulence, and thermal blooming effect is all related to the main laser wavelength. Atmospheric optical parameters in Easylaser have multiple wavelength profiles that vary with altitude, which affect the atmospheric transmittance of laser transmission. According to formulas (3) and (4), the commonly used Fried parameter r_0 to describe the turbulence intensity and the thermal distortion parameter N_D to characterize the thermal blooming intensity are both functions of wavelength. Therefore, the laser transmission wavelength is also one of the parameters that cannot be ignored. The effect of the laser wavelength on the power distribution to the target spot is shown in Fig. 9.

As shown in Fig. 9, when the wavelength of the main laser is 0.88 um and 1.064um, the ring radius to the target spot is smaller and the power density is higher. The main reason is the combined influence of laser thermal blooming and diffraction effect, and a very small part is the influence of atmospheric turbulence and transmittance. The thermal blooming effect of the 0.88 um wavelength laser is more serious, but the diffraction angle is smaller, and adaptive optics can correct the thermal blooming to a certain extent. The laser thermal blooming effect at the wavelength of 1.064um is very small, almost negligible, but the diffraction angle is larger. As shown in Fig. 9 (b), the main laser wavelengths of 0.88umand 1.064 um have their own advantages in power density under the two different power ratios.

When we compare the power density under the power ratio of 0.6320, the main laser with wavelength of 0.88 um is slightly better than the main laser with wavelength of 1.064 um. When we compare the power density under the power ratio of 0.8378, the main laser with wavelength of 1.064um is better than the main laser with wavelength of 0.88um.

H. THE INFLUENCE OF ADAPTIVE OPTICS COMPENSATION ON THE POWER DISTRIBUTION TO THE TARGET SPOT

Adaptive optics compensation can increase the power density to the target spot, but its related parameters, such as the number of turns and arrangement of the deformable mirror driver, the number of Hartmann transverse elements, etc., will not have a great impact on the power distribution to the target spot. The numerical selection of more parameters only needs to be appropriate, and the values of these parameters are all derived from the relevant cases in Easylaser.

In order to analyze the changes brought by the adaptive optics system to the target power distribution, in the original laser transmission process model, the optical path is not changed, and the original tilting mirror and deformable mirror are replaced by reflecting mirrors. Other parameters are consistent with Table 1 and Table 3. We can compare the effect on the power distribution to the target spot with and without adaptive optics compensation, and calculate the power distribution to the target spot without turbulence and thermal blooming effects. Since its difference is relatively small, it is more suitable to be given in tabular form.

As shown in Table 4, when the laser slanted transmission is 4km, the power density of the power ratio 0.8378 differs by 188.1 w/cm^2 with and without adaptive optics compensation. It accounts for 3.23% of the power density under the power ratio 0.8378 without adaptive optics compensation. The power density of the power ratio 0.6320 differs by 100.38 w/cm^2 with and without adaptive optics compensation. It accounts for 3.30% of the power density under the power ratio 0.6320 without adaptive optics compensation.

The application scenario of this paper is the airborne laser high-altitude, close-range combat. The impact of atmospheric turbulence and thermal blooming effect cannot be ignored. The adaptive optics system can increase the power density to the target spot. As the transmission distance increases, the end of the laser is closer to the ground, and the turbulence and thermal blooming effects are more seriously affected. At this time, the effect of adaptive optics compensation is more obvious. It can determine whether adaptive optics compensation is necessary according to the demand when the airborne laser uses low power to strike targets within 2 km.

V. SUMMARY

Through numerical simulation, this paper analyzes the influence of airborne laser system parameters, transmission path parameters and atmospheric mode on the power distribution to the target spot, and the sensitivity analysis about some important parameters are also performed. Under the boundary conditions described in the above basic models, the response sensitivity can be compared and the sensitivity ranking is

$$S_{tracking\ accuracy(1\mathrm{urad})} > S_{laseremissionaperture(0.1\mathrm{m})} > S_{transmission\ distance(300\mathrm{m})} > S_{lasersourcepoewer(10\mathrm{kw})},$$

which is consistent under the two different power ratios. It can provide a basis for the parameter design of airborne laser in the future high-altitude and close-range combat scenarios.

When analyzing the influence of the adaptive optics system on the power density to the target spot, the detailed value of the power density to the target spot is given in this paper. Although the high-altitude atmosphere is clean, the influence of atmospheric turbulence and thermal blooming effect on the laser cannot be ignored, and the adaptive optics system can compensate for the atmospheric effect to a certain extent.

In future work, it will be possible to build a full link simulation model of laser operational scenarios, laser transmission and laser thermal damage to achieve operational effectiveness analysis. The calculation method of laser transmission can provide a reference in other laser operational scenarios. The results of operational effectiveness analysis can provide a theoretical basis for the parameter design of actual equipment systems in the future.

REFERENCES

[1] H. Kaushal and G. Kaddoum, "Applications of lasers for tactical military operations," *IEEE Access*, vol. 5, pp. 20736–20753, 2017, doi: 10.1109/ACCESS.2017.2755678.

[2] Y. Ding, F. Jiang, R. Zheng, and J, Zhang, "Overview of high energy laser weapon development in USA (Invited)," *Electro-Optic Technol. Appl*, vol. 36, no. 6, pp. 1–9, Dec. 2021.

[3] H. Wang, "Analysis on the key technologies and typical battle mode of laser weapon," *Aero Weaponry*, vol. 27, no. 2, pp. 25–31, Dec. 2019, doi: 10.12132/ISSN.1673-5048.2019.0260.

[4] J. Yu. *Investigation Report on the Current Situation and Development Trend of Laser Weapons at Home and Abroad*. Beijing sun valley consulting.ltd. Beijing, China. Accessed: Mar. 18, 2022. [Online]. Available: https://maimai.cn/article/detail?fid=1607795674&efid=R5fmzHyfcF0tbb1LDsCsyQ

[5] Y. Yue, X. Xie, J. Zhang, J. An, and F. Zhang, "Research of beam control system component simulation and separation method of the kinematics coupling," *High Power Laser Part Beams*, vol. 26, no. 9, pp. 1–9, Sep. 2014, doi: 10.1117/12.2065400.

[6] M. C. Azar, "Assessing the treatment of airborne tactical high energy lasers in combat simulations," M.S. thesis, Air Force Inst. Technol., Sperlins, CO, USA, 2003.

[7] A. Lionis, "Experimental design of a UCAV-based high-energy laser weapon," M.S. thesis, Navy Postgraduate School, Monterey, CA, USA, 2016.

[8] M. P. Melin, "Modeling and Analysis of High Energy Laser Weapon System Performance in Varying Atmospheric Conditions," M.S. thesis, Air Force Inst. Technol., Sperlins, CO, USA, 2011.

[9] M. Xu, Y. Sun, T. Wang, and R. Li, "Application and effect analysis of high power laser atmospheric transmission," *Proc. SPIE*, vol. 11763, Mar. 2021, Art. no. 117633M, doi: 10.1117/12.2586624.

[10] Q. Yun, B. Song, and Y. Pei, "Modeling the impact of high energy laser weapon on the mission effectiveness of unmanned combat aerial vehicles," *IEEE Access*, vol. 8, pp. 32246–32257, 2020, doi: 10.1109/ACCESS.2020.2973492.

[11] Q. Zhao, H. Fan, and Y. Li, "Simulation and experimental study about hollow high energy laser propagating through atmosphere," *Laser Technol.*, vol. 38, no. 4, pp. 542–545, doi: 10.7510/jgjs.issn.1001-3806.2014.04.021.

[12] C. Yin, "Laser indoor simulation experiments of thermal blooming and turbulence effects," M.S. thesis, School Phys. Optoelectron. Eng., Xidian Univ., Xi'an, China, 2019.

[13] Y. Gao, X. Gao, Y. Wu, C. Zhang, and L. Zhang, "Application of liquid crystal spatial light modulator in university optical experiment," *Phys. Exp. College*, vol. 34, no. 6, pp. 45–48, Dec. 2021, doi: 10.14139/j.cnki.cn22-1228.2021.06.011.

[14] Y. Kong, X. Xu, and X. Ni, "Calculation of liquid crystal wave-front generation atmospheric turbulence simulator based on GPU," *Infr. Laser Eng.*, vol. 43, no. 9, pp. 3061–3065, Sep. 2014.

[15] X. Ding, "Study of atmospheric turbulence simulator using fractal method," M.S. thesis, School Phys. Optoelectron. Eng., Taiyuan Univ. Technol., Taiyuan, China, 2014.

[16] B. Hu, "Analysis on high-energy laser atmospheric transmission characteristic and adaptive optics technology," *Electro-Optic Technol. Appl.*, vol. 73, no. 5, pp. 7–10, Oct. 2003.

[17] S. Wu, X. Li, and X. Luo, "Numerical simulation of horizontal propagation steady-state thermal blooming effect on laser beam with different intensity distribution," *Opto-Electron. Eng.*, vol. 45, no. 2, pp. 53–65, 2018, doi: 10.12086/oee.2018.170620.

[18] X. Xie, J. Zhang, Y. Yue, J. An, and F. Zhang, "EasyLaser: Component-based laser system simulation software," *High Power Laser Part Beams*, vol. 25, no. 10, pp. 2536–2540, Oct. 2013, doi: 10.3788/HPLPB20132510.2536.

[19] H. Chen, Y. Chen, and Y. Li, "Simulation of atmospheric transmission characteristics of laser at 1.06 μm," *Laser Technol.*, vol. 38, no. 2, pp. 266–269, 2014, doi: 10.7510/jgjs.issn.1001-3806.2014.02.025.

[20] H. Dong, W. Li, and M. Dai, "Research of high power fiber laser atmosphere propagation," *Opt. Technique*, vol. 33, no. 6, pp. 830–832, 2007, doi: 10.1002/jrs.1570.

[21] P. M. Lushnikov and N. Vladimirova, "Toward defeating diffraction and randomness for laser beam propagation in turbulent atmosphere," *JETP Lett.*, vol. 108, no. 9, pp. 571–576, Nov. 2018, doi: 10.1134/s0021364018210026.

[22] Z. Ding, X. Li, and J. Cao, "Thermal blooming effect of Hermite–Gaussian beams propagating through the atmosphere," *J. Opt. Soc. Amer. A, Opt. Image Sci.*, vol. 36, no. 7, pp. 1152–1160, 2019, doi: 10.1364/JOSAA.36.001152.

[23] *User Manual of Simulation Software EasyLaser*, China Academy of Engineering Physics, Beijing, China, 2018.

[24] Q. CAO, J. Lu, J. Liu, and J. Yan, "From SHiELD to look into the anti-missile capability and technical challenge of airborne laser weapon," *J. Chin. Acad. Electron. Sci.*, vol. 14, no. 5, pp. 443–451, Dec. 2019, doi: 10.3969/j.issn.1673-5692.2019.05.001.

[25] (2022). *Ordnance Industry Science Technology*. Shaanxi Association for Science and Technology. Accessed: Mar. 14, 2022. [Online]. Available: https://baijiahao.baidu.com/s?id=1731781115821608515&wfr=spider&for=pc

[26] Z. Huang, Y. Feng, and Y, Lu, "Development of airborne electro-optical targeting systems abroad," *Electron.-Optics Control*, vol. 28, no. 10, pp. 61–66, Dec. 2021, doi: 10.3969/j.issn.1671-637X.2021.10.013.

[27] Z. Du, H. Tang, K. Liu, and S. Chen, "Development and flight test characteristics of Israeli's airborne laser weapon," *Laser Infr.*, vol. 51, no. 12, pp. 1547–1553, Dec. 2021, doi: 10.3969/j.issn.1001-5078.2021.12.001.

[28] D. Zhang, X. Li, Y. Huang, and J. Wang, "Analysis of damage effect of U.S. Army ground-based laser against cruise missile," *Mod. Defence Technol.*, vol. 41, no. 6, pp. 8–13, Dec. 2013, doi: 10.3969/j.issn.1009-086x.2013.06.002.

[29] J. Zhang, F. Zhang, and Y. Wu, "Methods for simulating turbulent phase screen," *High Power Laser Part. Beams*, vol. 24, no. 10, pp. 2318–2324, 2012, doi: 10.3788/HPLPB20122410.2318.

[30] Y. Li, W. Zhu, and R. Rao, "Simulation of random phase screen of non-Kolmogorov atmospheric turbulence," *Infr. Laser Eng.*, vol. 45, no. 12, pp. 169–176, Dec. 2016, doi: 10.3788/IRLA201645.1211001.

[31] J. Zhang, F. Zhang, H. Su, P. Hu, X. Xie, and W. Luo, "Analysis of beam deviation induced by thermal blooming effect when high-energy laser propagating up in atmosphere," *Acta Physica Sinica*, vol. 70, no. 24, pp. 128–134, Sep. 2021, doi: 10.7498/aps.70.20211138.

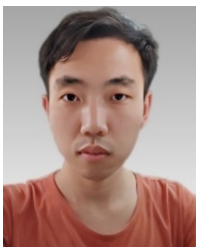

LE LIU received the B.S. degree in solution of light wave mode of laser resonator from Hubei Normal University, in 2020. He is currently pursuing the M.S. degree in parameter design of airborne laser with the Changchun Institute of Optics, Fine Mechanics and Physics, CAS, China. His research interests include agent-based modeling and simulation, laser transmission, laser thermal damage, and combat effectiveness analysis.

CHENYANG XU, photograph and biography not available at the time of publication.

WENBIN ZENG, photograph and biography not available at the time of publication.

BAOKU LI, photograph and biography not available at the time of publication.

JIN GUO, photograph and biography not available at the time of publication.

SHENG CAI received the B.S. degree from the Huazhong University of Science and Technology, Wuhan, Hubei, in 2005, and the Ph.D. degree from the Changchun Institute of Optics, Fine Mechanics and Physics, CAS, China, in 2010. He is currently a Master Tutor, a Professor, and a member of the Youth Innovation Promotion Association, CAS. His research interests include opto-electronic situational awareness and countermeasure.